LANGMUIR

Article

pubs.acs.org/Langmuir

Tuning Band Structure of Cadmium Chalcogenide Nanoflake Arrays via Alloying for Efficient Photoelectrochemical Hydrogen Evolution

Yan Zhang,[†,‡] Peng-Fei Yin,[†] Xiao-Hua Liu,[†] Jing Mao,[†] Sergei A. Kulinich,*[,§] and Xi-Wen Du*[,†,‡]

[†]Institute of New-Energy Materials, School of Materials Science and Engineering and [‡]Key Laboratory of Advanced Ceramics and Machining Technology, Ministry of Education, Tianjin University, Tianjin 300072, China

[§]Institute of Innovative Science and Technology, Tokai University, Hiratsuka, Kanagawa 259-1292, Japan

Supporting Information

ABSTRACT: Owing to their high extinction coefficient and moderate band gap, cadmium chalcogenides are known as common semiconductors for photoelectric conversion. Nevertheless, no ideal cadmium chalcogenide with proper band structure is available yet for photoelectrochemical hydrogen evolution. In this work, we modified the band structure of CdTe via alloying with Se to achieve a ternary compound ($CdSe_{0.8}Te_{0.2}$) with n-type conduction, a narrower band gap, and a more negative band position compared to those of CdSe and CdTe. This novel material exhibits strong light absorption over a wider spectrum range and generates more vigorous electrons for hydrogen reduction. As a result, a photoelectrode based on nanoflake arrays of the new material could achieve a photocurrent density 2 times that of its CdSe counterpart, outperforming similar materials previously reported in the literature. Moreover, the quick transfer of holes achieved in the novel material was found to depress photocorrosion processes, which led to improved long-term working stability.

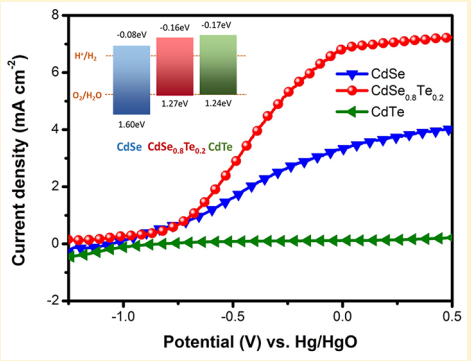

1. INTRODUCTION

Hydrogen, as a clean and efficient energy source, is an ideal solution to the energy shortage and environment related issues. As an effective way to obtain hydrogen and because of their direct use of solar energy, photoelectrochemical (PEC) hydrogen evolution processes have attracted much attention since the discovery of the Honda-Fujishima effect in 1972.[1]

Making a high-performance photoanode is known as one of the key points in achieving PEC cells with high solar-to-hydrogen (STH) conversion.[2−5] An efficient photoanode should meet the following three requirements. (1) It should be based on an n-type semiconductor, with the majority of its carriers being electrons that can move quickly to the counter electrode and avoid any recombination.[6] (2) Its band gap should be appropriate for highly efficient light harvesting, implying both efficient light absorption and efficient carrier separation.[7] (3) Its conduction band should be high enough for excited electrons to reduce protons adsorbed on the electrode.[8]

Among semiconductors commonly used in photoelectric conversion, cadmium chalcogenides such as CdS,[9−11] CdSe,[12−14] and CdTe[15] have attracted significant attention because of their high extinction coefficient, moderate band gap, and proper band structure. Of these three, CdTe has been extensively applied in thin-film and quantum-dot solar cells, exhibiting ultrahigh light-harvesting efficiency (LHE) resulting from its narrow band gap (1.4 eV). However, its p-type character and low conduction band hinder its application in PEC hydrogen evolution. A possible solution would be to adjust the conduction type of CdTe material via alloying while keeping its band gap unchanged. For example, CdTe could be alloyed with CdSe so that a ternary compound with n-type conduction, a narrow band gap, and proper band position is achieved.[16]

Apart from the material type and properties, the morphology of the photoanode also plays a key role in its performance. Three-dimensional (3D) structures such as nanorod arrays[17−19] and inverse opal[11,20−22] were previously reported as those enhancing light absorption and improving the photocurrent. Recently, we found that another nanostructure, nanoflake arrays (NFAs), can also be attractive for photoelectric and photoelectronic applications (Figure 1).[23] First, NFAs exhibit an intriguing light-trapping effect, as incident light can be reflected many times and thus entirely absorbed by them, which is expected to increase their LHE tremendously. Second, thin nanoflakes provide a shortcut for the diffusion of minority carriers to the surface, which can accelerate charge separation and the transportation of minority carriers along the thickness direction. Third, vertical nanoflakes can provide a quick path for electron flow, reducing possible losses of carriers. Forth, the large specific surface of NFAs should facilitate their contact with electrolytes, expediting the consumption of minority carriers and reducing their accumulation.[24−26]

On the basis of the above considerations, in the present study, we attempted to engineer an anode based on n-type

Received: March 15, 2017
Revised: June 8, 2017
Published: June 14, 2017

DOI: 10.1021/acs.langmuir.7b00878
Langmuir 2017, 33, 6457−6463

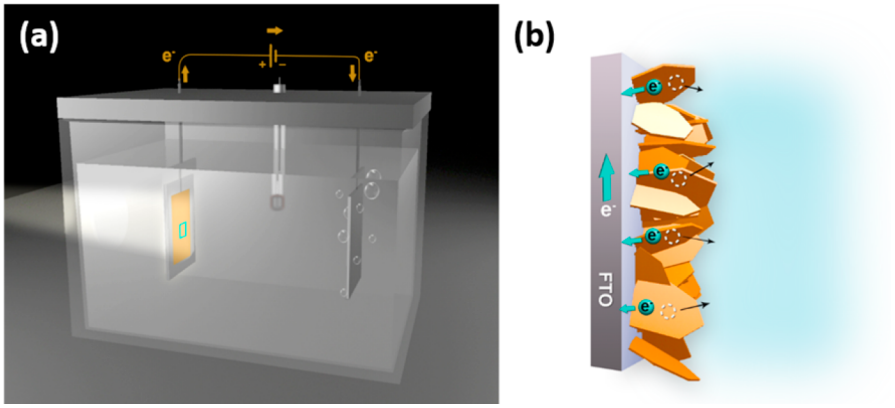

Figure 1. (a) Experimental setup for PEC water splitting and (b) schematic structure of the photoanode based on NFAs developed in this study.

semiconductor NFAs with a composition of $CdSe_{0.8}Te_{0.2}$. Although $CdSe_xTe_{1-x}$ materials have been widely used as efficient light absorbers,[27,28] their application for PEC hydrogen evolution has not been reported. We first synthesized Cd NFAs by thermal evaporation and then converted them into CdSe NFAs via a gas-phase selenization process, after which the CdSe NFAs were alloyed through anion exchange. Upon subsequent annealing, the as-prepared $CdSe_{0.8}Te_{0.2}$ NFAs were applied to PEC water splitting and hydrogen evolution. The novel ternary photoanode achieved a photocurrent density of as high as 6.5 mA/cm^2, which was 2 times that of its CdSe counterpart. In contrast, CdTe NFAs with similar morphology showed no photocurrent under the same test conditions. The superior performance of the new photoanode is attributed to its n-type and improved light absorption by its NFAs. Our work demonstrates that energy band engineering is an effective strategy for photoanodes with high PEC performance.

2. EXPERIMENTAL SECTION

2.1. Chemicals. Cadmium sulfide (CdS, 98% purity), selenium powder (Se, −325 mesh particle size, 99.5% purity), tellurium powder (Te, −200 mesh particle size, 99% purity), sodium hydroxide (NaOH, 99% purity), and ethanol (C_2H_5OH, absolute) were purchased from Alfa Aesar and directly used without further treatment or purification. Hydrochloric acid (HCl, 38 wt %) was purchased from Jiangtian Chemical Technology Co., Ltd.

2.2. Preparation of the Cd NFA Template. The Cd NFAs were prepared using a CVD method previously reported elsewhere.[23] In brief, 0.15 g of CdS, as a Cd source, was placed into a quartz tube and then heated in the middle of the vacuum tube furnace. A slide of FTO glass, sputter-coated with an ultrathin TiO_2 layer as a buffer and a seed layer (which was used to prevent any electricity leaks during photoelectrochemical measurements), was put next to the furnace (downstream) as the substrate. N_2 (200 sccm) and air (40 sccm) were allowed to flow through the tube. During the deposition (30 min), the temperature was set at 650 °C and the pressure was kept at 8.5 Torr. During the temperature increase, the pressure was kept at 200 Torr. The as-deposited template was immersed in dilute NaOH (pH 9) to remove absorbed SO_2 generated during the formation of Cd NFAs and then rinsed with deionized water and kept for further experiments.

2.3. Preparation of CdSe and Alloyed NFAs. CdSe NFAs were prepared from the raw template via a gas-phase selenization process. Se powder (0.1 g) was put in the middle of a quartz tube, which was then placed into a vacuum tube furnace, while the template with Cd NFAs was set downstream, next to the tube. The furnace was heated to 300 °C for 30 min while N_2 flowed at 30 sccm at a pressure of 2.5 Torr. The as-prepared CdSe NFAs were then annealed at 500 °C in N_2 to get rid of residual raw materials and reduce the number of defects.

As the final stage, $CdSe_{0.8}Te_{0.2}$ NFAs were prepared through partial gas-phase anion exchange reported for the first time. For this, 0.1 g of Te powder was placed in the middle of the vacuum tube furnace while the sample with CdSe NFAs to be alloyed was placed downstream, next to the Te source. The reaction temperature was set at 500 °C, and 30 sccm of N_2 gas flowed for 15 min. Finally, the obtained $CdSe_{0.8}Te_{0.2}$ NFAs were annealed at 500 °C to get rid of residual raw materials and reduce the number of defects.

2.4. Preparation of CdTe NFAs. CdTe NFAs were prepared through a previously described put-in heating process.[29] In a few words, a one-end thin quartz tube was placed into a furnace tube with 0.05 g of Te powder set at the closed end and a sample with Cd NFAs kept at a distance of 10 cm. The whole system was evacuated and flushed with N_2 gas to remove residual oxygen. Then, the furnace was heated to 420 °C, after which the tube with initial materials was rapidly put into the furnace and kept there for 20 min under a continuous flow of N_2 (50 sccm).

2.5. Photoelectrochemical Measurements for Hydrogen Evolution. A standard three-electrode system was applied for PEC water splitting with the as-prepared materials as working electrodes, HgO/Hg in 1 M KOH solution as the reference electrode, and Pt foil as the counter electrode. The results were recorded with a Versastat3 potentiostat electrochemistry workstation. The whole system was placed under standard AM 1.5G solar illumination simulated by Xe light (Perfect Light Pls-sxe300c, 300 W) as shown in Figure 1. A solution of 0.25 M Na_2S/0.35 M Na_2SO_3 was used as the electrolyte and sacrificial agent.

2.6. Characterization. Scanning electron microscopy (SEM, Hitachi S-4800 with accelerating voltage 5 kV) and transmission electron microscopy (TEM, Tecnai G2 F20 equipped with a field-emission gun operating at 200 kV) were used to acquire the morphology of each sample. An energy-dispersive spectroscopy (EDS) module attached to the TEM instrument was used to analyze the elemental composition. X-ray diffraction (XRD, Bruker-D8) analysis was applied to study the crystalline structure. Inductively coupled plasma−mass spectrometry (ICP−MS) measurements were acquired with an Agilent 7700X, and UV−vis absorption spectra were recorded with a Hitachi 4100 UV−vis absorption spectrometer. X-ray photoelectron spectroscopy (XPS) analyses were carried out with a PHI-1600 ESCA spectrometer (with a monochromatic Al Kα X-ray source, 1486.6 eV) to analyze the chemical composition and bonding states of elements. SEM, XRD, XPS, UV−vis absorption spectra and photoelectrochemical measurements were made using samples prepared on FTO, and TEM and EDS were performed with the product transferred onto Cu grids. Finally, for ICP-MS, NFAs were first dissolved in concentrated nitric acid at 150 °C and then diluted with deionized water to obtain the solution for analysis.

3. RESULT AND DISCUSSION

The top-view SEM images of three samples are presented in Figure 2a−c and Figure S1. As seen in Figure 2a, the Cd

DOI: 10.1021/acs.langmuir.7b00878
Langmuir 2017, 33, 6457−6463

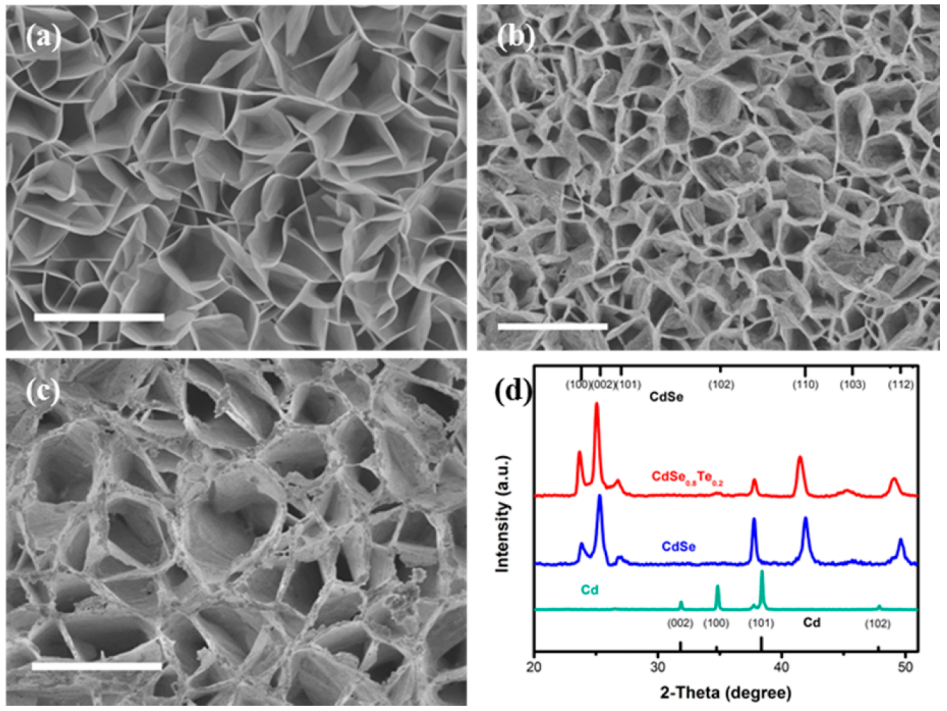

Figure 2. Morphology of initial Cd NFAs (a), CdSe NFAs (b), and $CdSe_{0.8}Te_{0.2}$ NFAs (c) and their XRD patterns (d). Scale bars in (a–c) indicate 10 μm.

Table 1. Peak Positions for Each Sample in the XRD Patterns and *x* Values Calculated from Them

	(100)		(002)		(110)		
sample	position/deg	spacing/Å	position/deg	spacing/Å	position/deg	spacing/Å	*x* value
CdSe	23.825	3.7317	25.339	3.5120	41.896	2.1545	1
$CdSe_{0.8}Te_{0.2}$	23.681	3.7581	25.056	3.5546	41.485	2.1814	0.8
CdTe	22.319	3.9800	23.707	3.7500	39.222	2.2950	0

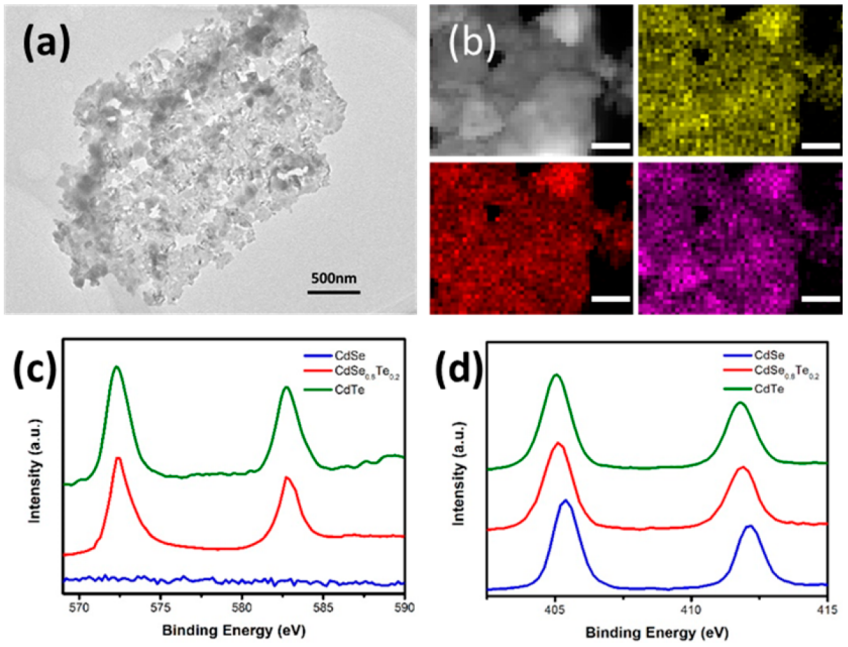

Figure 3. (a) TEM image of a single $CdSe_{0.8}Te_{0.2}$ nanoflake. (b) Higher-resolution TEM image of the flake and corresponding elemental mapping for three detected elements: Cd (yellow), Se (red), and Te (purple). Scale bars in (b) indicate 50 nm. (c, d) Narrow-scan XPS Te 3d and Cd 3d spectra, respectively, for CdSe, CdTe, and $CdSe_{0.8}Te_{0.2}$ NFA samples. Corresponding survey-scan spectra of the same samples as well as narrow-scan Se 3d spectra are shown in Figure S10.

DOI: 10.1021/acs.langmuir.7b00878
Langmuir 2017, 33, 6457–6463

nanoflakes grew vertically on the substrate and formed a network of arrays. The latter NFA morphology was preserved after ion exchange and annealing, when CdSe and $CdSe_{0.8}Te_{0.2}$ materials formed (Figure 2b,c). The height of nanoflakes over the substrate was about 8 μm, according to the cross-sectional SEM image in Figure S2. The XRD patterns shown in Figure 2d indicate that the Cd, CdSe, and $CdSe_{0.8}Te_{0.2}$ NFAs possess hexagonal wurtzite phase structure, whereas the CdTe NFAs have zinc-blende phase structure (Figure S5). The HRTEM image and corresponding fast Fourier transformation (FFT) pattern confirm that the $CdSe_{0.8}Te_{0.2}$ product obtained after ion exchange inherited the crystal structure of CdSe NFAs (Figure S3). The interplanar spacings for three main crystal planes deduced from XRD patterns are presented in Table 1. According to Vegard's law, the alloy lattice constant of $CdSe_xTe_{1-x}$ varies linearly with x;[30] therefore, the x value can be deduced from the XRD results through simple interpolation. According to the results shown in Table 1, the $CdSe_xTe_{1-x}$ alloy material prepared in this study possessed an x value of about 0.8. This value is consistent with the composition derived from ICP−MS results, which demonstrated atomic ratio Cd/Se/Te to be 1:0.76:0.21, as well as with EDS results (Figure S4), which showed the contents of Cd, Se, and Te to be 53.5, 37.1, and 9.4 atom %, respectively. In parallel, another alloy with the composition of $CdSe_{0.63}Te_{0.37}$ was also prepared to demonstrate the effect of reaction time during anion exchange on the composition of the final product (Figure S6).

The bright-field TEM image in Figure 3a indicates that each individual nanoflake has pores of several tens of nanometers in size. A high-angle annular dark-field (HAADF) TEM image and corresponding elemental distribution are shown in Figure 3b. The HAADF image illustrates that the nanoflake consists of tiny particles, thus being polycrystalline in nature. In the elemental mapping images (Figure 3b), Cd, Se, and Te are all distributed homogeneously, suggesting a pure alloy phase without phase separation or element segregation.

The bonding states of each element in the novel semiconductor material were characterized by XPS (spectra presented in Figure 3c,d and Figure S10b). The peak located at 54.4 eV (Figure S10b) is characteristic of Se^{2-} anions,[31] and the two peaks centered at 572.4 and 583.1 eV observed in Figure 3c indicate the presence of Te^{2-} anions.[32] The Cd 3d peak positions in Figure 3d are seen to shift gradually from 405.8 and 412.2 eV (CdSe) to 405.3 and 412.0 eV ($CdSe_{0.8}Te_{0.2}$) and then to 405.1 and 411.8 eV (CdTe),[31,32] suggesting that Te atoms with lower electronegativity gradually substitute for Se atoms in the semiconductor materials.

The prepared sample with $CdSe_{0.8}Te_{0.2}$ NFAs was evaluated as a photoanode for PEC hydrogen evolution and tested in a standard three-electrode system under solar illumination of AM 1.5 as shown in Figure 1. The CdSe and CdTe samples prepared using similar Cd NFA templates were also evaluated for comparison. Figure 4a displays the current density−potential (J−V) curves recorded both in the dark and under illumination. The $CdSe_{0.8}Te_{0.2}$ photoanode demonstrated higher values of the photocurrent density (red symbols in Figure 4a) than did its CdSe counterpart. At 0 V vs the Hg/HgO reference, the newly developed alloy electrode achieved a photocurrent density of 6.8 mA/cm^2, which was almost 2 times larger than that of the CdSe electrode (4 mA/cm^2). At the same time, the CdTe electrode showed practically no photocurrent in the region. The other alloyed photoanode (with a composition of $CdSe_{0.63}Te_{0.37}$) had a much lower

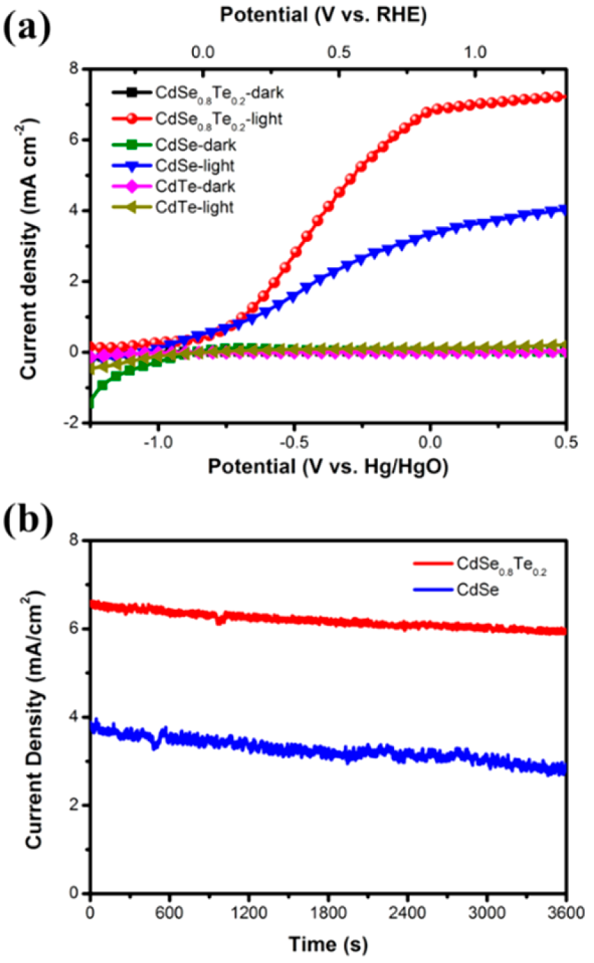

Figure 4. PEC performance of three semiconductor photoanodes. (a) Linear sweep voltammetry measurements of electrodes with CdSe, CdTe, and $CdSe_{0.8}Te_{0.2}$ NFAs under 1 sun AM 1.5G illumination and in the dark. (b) Photocurrent stability of CdSe and $CdSe_{0.8}Te_{0.2}$ electrodes under 1 sun AM 1.5G illumination and at 0 V vs the Hg/HgO reference electrode.

current density (Figure S6b), which is why it was not studied in greater detail in the present work. The plateau photocurrent exhibited by the $CdSe_{0.8}Te_{0.2}$ electrode in Figure 4a is believed to arise from its better electron conductivity compared to that of the CdSe electrode. The stability of the CdSe and $CdSe_{0.8}Te_{0.2}$ electrodes during their performance was evaluated at 0 V vs Hg/HgO under continuous illumination of AM 1.5, with the results shown in Figure 4b and Figure S7. The photocurrent density−time (J−t) curve of the alloyed electrode proves to be more stable: only an ∼10% decay during nonstop 1 h measurement was observed, whereas the performance of the CdSe electrode degraded by about 25% during the same testing period. The experimentally measured quantities of produced hydrogen matched very well those calculated assuming 100% Faradaic efficiency (Figure S8), indicating that almost all photoelectrons produced by the alloyed electrode contributed to hydrogen reduction.

To understand the reasons behind the excellent PEC performance demonstrated by the ternary chalcogenide NFAs, we applied a variety of techniques to analyze how the three electrodes worked. First, we compared how the three photoelectrodes absorbed light. The LHE plots presented in Figure 5a were calculated by subtracting the reflected and

DOI: 10.1021/acs.langmuir.7b00878
Langmuir 2017, 33, 6457−6463

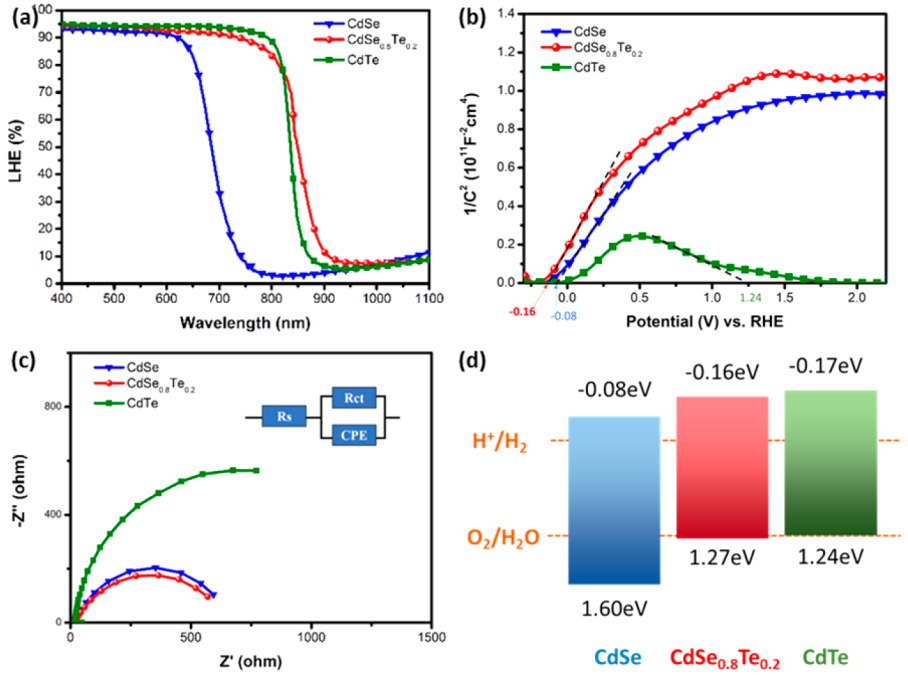

Figure 5. Light absorption and PEC hydrogen evolution performance of three chalcogenide NFAs. (a) LHE, (b) the Mott–Schottky curves in the dark, and (c) EIS under AM 1.5G illumination for the three samples. CdSe, CdTe, and $CdSe_{0.8}Te_{0.2}$ are presented by blue, green, and red lines, respectively. (d) Scheme for the devices' energy level for each photoanode.[37,38,41,42]

transmitted light from the total incident light (Figure S11). The observed results demonstrated the absorption efficiency above 90% over the visible light region for all three samples. This implies that the NFAs trap light very efficiently, which agrees well with what was previously reported for CdS NFAs.[23] The absorption band edge for $CdSe_{0.8}Te_{0.2}$ is located at 930 nm, and those for CdTe and CdSe are blue-shifted by 40 and 180 nm, respectively (Figure 5a), suggesting that the ternary electrode could absorb light within a somewhat broader wavelength range. The UV–vis absorption spectroscopy and corresponding Tauc plots (Figure S12) reveal that a narrower band gap (1.43 eV) was achieved for the ternary semiconductor compared to its binary counterparts (1.48 eV for CdTe and 1.68 eV for CdSe). The narrowing band gap that was found is believed to result from the disordered crystal lattice caused by mixed anions, which was previously proven both theoretically[33,34] and experimentally.[35,36]

The Mott–Schottky (M–S) analysis was carried out to determine the p/n type of the samples. Both the CdSe and $CdSe_{0.8}Te_{0.2}$ NFA anodes showed positive slopes in their plots, which indicated that electrons were their major carriers (Figure 5b). This implies that these two materials are n-type semiconductors. In addition, the flat-band potential, which is determined by the tangent line of the plot, was −0.16 and −0.08 V for the $CdSe_{0.8}Te_{0.2}$ and CdSe samples, respectively, being in agreement with the literature[37,38] and showing that the novel $CdSe_{0.8}Te_{0.2}$ material had a more negative conduction band edge. Meanwhile, their slopes were almost the same (red and blue curves in Figure 5b), which means that the carrier concentration in the two samples was close, at least of the same order of magnitude. The M–S plot for the CdTe sample showed an asymmetric peak (green curve in Figure 5b), with its right shoulder having a lower slope than the left side. This implies that the major carriers in the CdTe material are holes,[39] with the sample being a p-type semiconductor with a flat-band potential of 1.75 eV, in good agreement with previous reports.[40−42]

Charge separation dynamics in the three photoanodes was characterized by electrochemical impedance spectroscopy (EIS). Figure 5c shows the Nyquist plots tested at 0 V vs Hg/HgO and under illumination of AM 1.5. The corresponding equivalent circuit model is shown in the inset of Figure 5c, where R_s is the electrolyte resistance, CPE is the constant phase element, and R_{ct} is the charge-transfer resistance between the photoanode and the electrolyte. By fitting the Nyquist plots with the given model, the values of R_{ct} for the CdSe and $CdSe_{0.8}Te_{0.2}$ electrodes were determined to be 655 and 621 Ω, respectively. This indicates that the rate of holes reacting with electrolyte on the surface of the two electrodes was almost at the same level. The rapid charge separation taking place in the two electrodes was also proven by open circuit photovoltage decay spectra (Figure S13). Compared to the CdTe material (1541 Ω), the reaction between holes and electrolyte was more favorable for these two electrodes. The reason might be that the valence band position of the CdTe material is more positive, which slows down the reaction kinetics.

On the basis of the above results, the novel ternary photoelectrode reported here demonstrates several attractive features that contribute to its superior performance during PEC hydrogen evolution. As was mentioned above, the band structure of the photoelectrode plays a crucial role in its performance. According to the light absorption spectra and the flat-band potentials derived from the M–S curves, the band structures of the samples are shown in Figure 5d. Among the three semiconductors, the $CdSe_{0.8}Te_{0.2}$ anode exhibits the narrowest band gap. Its relatively narrow band gap can improve light harvesting and generate more photocarriers. At the same time, its negative conduction band edge (−0.16 eV, Figure 5d) should lead to photoelectrons with higher energy, also speeding up reactions related to hydrogen generation. Therefore, the

DOI: 10.1021/acs.langmuir.7b00878
Langmuir 2017, 33, 6457−6463

$CdSe_{0.8}Te_{0.2}$ material can produce many more electrons with higher energy than its counterparts with CdSe and CdTe NFAs. Meanwhile, doping CdSe with Te atoms does not cause any recombination centers or deteriorated charge separation. Therefore, the $CdSe_{0.8}Te_{0.2}$ photoanode achieves a photocurrent about 2 times larger than that of its CdSe counterpart. As for the poor PEC performance of the CdTe material, p-type semiconductors are known to be unfavorable for electron transfer because electrons are minor carriers in such materials.

Regarding long-term durability, photoelectrodes are often known to suffer from photocorrosion (caused by accumulated holes), which proceeds through the following reaction:[43]

$$CdX + 2h^+ \rightarrow Cd^{2+} + X^0 \ (X = Se, Te)$$

In the $CdSe_{0.8}Te_{0.2}$ and CdSe NFAs, some hole accumulation was proven by sharp spikes in the photocurrent transient response (Figure S14).[44] Nevertheless, the charge-transfer resistance of the $CdSe_{0.8}Te_{0.2}$ sample (621 Ω) was somewhat lower than that of the CdSe material (655 Ω) while being much lower than that of CdTe (1541 Ω). As a result, the $CdSe_{0.8}Te_{0.2}$ photoanode exhibited the best stability. Its thin-nanoflake structure provided a shortcut for hole diffusion, and it reacted with electrolyte, giving rise to the superior long-term durability of the novel material when compared to similar materials reported in the literature.[12−14]

4. CONCLUSIONS

We report on ternary $CdSe_{0.8}Te_{0.2}$ nanoflake arrays prepared via anion exchange that demonstrate high performance as photoanodes for photoelectrochemical water splitting. Owing to the band gap bowing effect caused by alloying, light absorption of the new material was expanded to a wider range and its photogenerated electrons were more energetic for hydrogen reduction. As a result, the as-prepared $CdSe_{0.8}Te_{0.2}$ photoelectrode could achieve a photocurrent density almost 2 times that of its CdSe counterpart, outperforming similar materials previously reported in the literature. Moreover, the quick transfer of holes achieved in the novel material was found to depress photocorrosion processes, which led to improved long-term working stability. The results suggest that the simple fabrication method described in this work provides an efficient way to prepare ternary semiconductors that are promising as photoanodes for photoelectrochemical systems designed for hydrogen evolution.

■ ASSOCIATED CONTENT

Supporting Information

The Supporting Information is available free of charge on the ACS Publications website at DOI: 10.1021/acs.langmuir.7b00878.

Top-view SEM image of CdTe NFAs. Cross-sectional SEM image of Cd NFAs. HRTEM image of a single $CdSe_{0.8}Te_{0.2}$ nanoflake. EDS spectrum of a $CdSe_{0.8}Te_{0.2}$ sample. XRD pattern of a CdTe sample. XRD pattern of a $CdSe_{0.63}Te_{0.37}$ sample with the corresponding linear sweep voltammetry measurements of $CdSe_{0.63}Te_{0.37}$ NFAs. Long-term stability of a $CdSe_{0.8}Te_{0.2}$ sample. Gas chromatography spectrum recorded with the product obtained using the photoelectrochemical system. Hydrogen evolution of the $CdSe_{0.8}Te_{0.2}$ photoanode over time. Photoconversion efficiency versus bias potential under solar illumination. Survey-scan and narrow-scan XPS spectra. Light absorption by the three samples. UV−vis absorption spectra and Tauc plots calculated from UV−vis−NIR absorption for NFA samples. Open circuit photovoltage decay spectra of electrodes. Current−time curve under chopped light illumination for NFAs. (PDF)

■ AUTHOR INFORMATION

Corresponding Authors

*E-mail: skulinich@tokai-u.jp.
*E-mail: xwdu@tju.edu.cn.

ORCID

Sergei A. Kulinich: 0000-0002-1365-9221
Xi-Wen Du: 0000-0002-2811-147X

Notes

The authors declare no competing financial interest.

■ ACKNOWLEDGMENTS

This work was supported by the National Basic Research Program of China (2014CB931703), the Natural Science Foundation of China (51571149 and 51471115), and the Natural Science Foundation of Tianjin City (15JCYBJC18200).

■ REFERENCES

(1) Fujishima, A.; Honda, K. Electrochemical Photolysis of Water at a Semiconductor Electrode. *Nature* **1972**, *238*, 37−38.

(2) Yang, J.; Bao, C. X.; Yu, T.; Hu, Y. F.; Luo, W. J.; Zhu, W. D.; Fu, G.; Li, Z. S.; Gao, H.; Li, F. M.; Zou, Z. G. Enhanced Performance of Photoelectrochemical Water Splitting with ITO@α-Fe_2O_3 Core-Shell Nanowire Array as Photoanode. *ACS Appl. Mater. Interfaces* **2015**, *7*, 26482−26490.

(3) Morales-Guio, C. G.; Liardet, C. G.; Mayer, M. T.; Tilley, S. D.; Gratzel, M.; Hu, X. L. Photoelectrochemical Hydrogen Production in Alkaline Solutions Using Cu_2O Coated with Earth-Abundant Hydrogen Evolution Catalysts. *Angew. Chem., Int. Ed.* **2015**, *54*, 664−667.

(4) Shan, L. W.; He, L. Q.; Suriyaprakash, J.; Yang, L. X. Photoelectrochemical (PEC) Water Oplitting of BiOI{001} Nanosheets Synthesized by a Simple Chemical Transformation. *J. Alloys Compd.* **2016**, *665*, 158−164.

(5) Emin, S.; de Respinis, M.; Fanetti, M.; Smith, W.; Valant, M.; Dam, B. A Simple Route For Preparation of Textured WO3 Thin Films from Colloidal W Nanoparticles and Their Photoelectrochemical Water Splitting Properties. *Appl. Catal., B* **2015**, *166*, 406−412.

(6) Chen, X. P.; Zhang, Z. X.; Chi, L. N.; Nair, A. K.; Shangguan, W. F.; Jiang, Z. Recent Advances in Visible-Light-Driven Photoelectrochemical Water Splitting: Catalyst Nanostructures and Reaction Systems. *Nano-Micro Lett.* **2016**, *8*, 1−12.

(7) Zeng, Q. Y.; Bai, J.; Li, J. H.; Li, Y. P.; Li, X. J.; Zhou, B. X. Combined Nanostructured Bi_2S_3/TNA Photoanode and Pt/SiPVC Photocathode for Efficient Self-Biasing Photoelectrochemical Hydrogen and Electricity Generation. *Nano Energy* **2014**, *9*, 152−160.

(8) Hisatomi, T.; Kubota, J.; Domen, K. Recent Advances in Semiconductors for Photocatalytic and Photoelectrochemical Water Splitting. *Chem. Soc. Rev.* **2014**, *43*, 7520−7535.

(9) Han, S. C.; Pu, Y. C.; Zheng, L. X.; Hu, L. F.; Zhang, J. Z.; Fang, X. S. Uniform Carbon-Coated CdS Core-Shell Nanostructures: Synthesis, Ultrafast Charge Carrier Dynamics, and Photoelectrochemical Water Splitting. *J. Mater. Chem. A* **2016**, *4*, 1078−1086.

(10) Ai, G. J.; Li, H. X.; Liu, S. P.; Mo, R.; Zhong, J. X. Solar Water Splitting by TiO_2/CdS/Co-Pi Nanowire Array Photoanode Enhanced with Co-Pi as Hole Transfer Relay and CdS as Light Absorber. *Adv. Funct. Mater.* **2015**, *25*, 5706−5713.

(11) Lu, Y. R.; Yin, P. F.; Mao, J.; Ning, M. J.; Zhou, Y. Z.; Dong, C. K.; Ling, T.; Du, X. W. A Stable Inverse Opal Structure of Cadmium Chalcogenide for Efficient Water Splitting. *J. Mater. Chem. A* **2015**, *3*, 18521−18527.

DOI: 10.1021/acs.langmuir.7b00878
Langmuir 2017, 33, 6457−6463

(12) Li, J.; Gao, X.; Liu, B.; Feng, Q. L.; Li, X. B.; Huang, M. Y.; Liu, Z. F.; Zhang, J.; Tung, C. H.; Wu, L. Z. Graphdiyne: A Metal-Free Material as Hole Transfer Layer to Fabricate Quantum Dot-Sensitized Photocathodes for Hydrogen Production. *J. Am. Chem. Soc.* **2016**, *138*, 3954−3957.
(13) Lee, J.; Cho, C. Y.; Lee, D. C.; Moon, J. H. Bilayer Quantum Dot-Decorated Mesoscopic Inverse Opals for High Volumetric Photoelectrochemical Water Splitting Efficiency. *RSC Adv.* **2016**, *6*, 8756−8762.
(14) Guo, M. M.; Wang, L. Y.; Xia, Y.; Huang, W.; Li, Z. L. Fabrication of Nano-CdSe Thin Films from Gas/Liquid Interface Reactions and Self-Assembly for Photoelectrochemical Hydrogen Production. *Int. J. Hydrogen Energy* **2016**, *41*, 2278−2284.
(15) Dong, Y. M.; Wu, R. X.; Jiang, P. P.; Wang, G. L.; Chen, Y. M.; Wu, X. M.; Zhang, C. Efficient Photoelectrochemical Hydrogen Generation from Water Using a Robust Photocathode Formed by CdTe QDs and Nickel Ion. *ACS Sustainable Chem. Eng.* **2015**, *3*, 2429−2434.
(16) Swartz, C. H.; Zaunbrecher, K. N.; Sohal, S.; LeBlanc, E. G.; Edirisooriya, M.; Ogedengbe, O. S.; Petersen, J. E.; Jayathilaka, P.; Myers, T. H.; Holtz, M. W.; Barnes, T. M. Factors Influencing Photoluminescence and Photocarrier Lifetime in CdSeTe/CdMgTe Double Heterostructures. *J. Appl. Phys.* **2016**, *120*, 165305.
(17) Duan, C. Y.; Wang, H.; Ou, X. M.; Li, F.; Zhang, X. H. Efficient Visible Light Photocatalyst Fabricated by Depositing Plasmonic Ag Nanoparticles on Conductive Polymer-Protected Si Nanowire Arrays for Photoelectrochemical Hydrogen Generation. *ACS Appl. Mater. Interfaces* **2014**, *6*, 9742−9750.
(18) AlOtaibi, B.; Nguyen, H. P. T.; Zhao, S.; Kibria, M. G.; Fan, S.; Mi, Z. Highly Stable Photoelectrochemical Water Splitting and Hydrogen Generation Using a Double-Band InGaN/GaN Core/Shell Nanowire Photoanode. *Nano Lett.* **2013**, *13*, 4356−4361.
(19) Garnett, E.; Yang, D. Light Trapping in Silicon Nanowire Solar Cells. *Nano Lett.* **2010**, *10*, 1082−1087.
(20) Kim, K.; Thiyagarajan, P.; Ahn, H. J.; Kim, S. I.; Jang, J. H. Optimization for Visible Light Photocatalytic Water Splitting: Gold-Coated and Surface-Textured TiO_2 Inverse Opal Nano-Networks. *Nanoscale* **2013**, *5*, 6254−6260.
(21) Ling, T.; Kulinich, S. A.; Zhu, Z. L.; Qiao, S. Z.; Du, X. W. Highly Conductive CdS Inverse Opals for Photochemical Solar Cells. *Adv. Funct. Mater.* **2014**, *24*, 707−715.
(22) Zheng, X. L.; Qin, W. J.; Ling, T.; Pan, C. F.; Du, X. W. Carbon Nanotube Reinforced CdSe Inverse Opal with Crack-Free Structure and High Conductivity for Photovoltaic Applications. *Adv. Mater. Interfaces* **2015**, *2*, 1400464.
(23) Yin, P. F.; Ling, T.; Lu, Y. R.; Xu, Z. W.; Qiao, S. Z.; Du, X. W. CdS Nanoflake Arrays for Highly Efficient Light Trapping. *Adv. Mater.* **2015**, *27*, 740−745.
(24) Li, Z. D.; Zhou, Y.; Xue, G. G.; Yu, T.; Liu, J. G.; Zou, Z. G. Fabrication of Hierarchically Assembled Microspheres Consisting of Nanoporous ZnO Nanosheets for High-Efficiency Dye-Sensitized Solar Cells. *J. Mater. Chem.* **2012**, *22*, 14341−14345.
(25) Qiu, Y. C.; Chen, W.; Yang, S. H. Facile Hydrothermal Preparation of Hierarchically Assembled, Porous Single-Crystalline ZnO Nanoplates and Their Application in Dye-Sensitized Solar Cells. *J. Mater. Chem.* **2010**, *20*, 1001−1006.
(26) Shi, Y. T.; Zhu, C.; Wang, L.; Li, W.; Cheng, C.; Ho, K. M.; Fung, K. K.; Wang, N. Optimizing Nanosheet-Based ZnO Hierarchical Structure through Ultrasonic-Assisted Precipitation for Remarkable Photovoltaic Enhancement in Quasi-Solid Dye-Sensitized Solar Cells. *J. Mater. Chem.* **2012**, *22*, 13097−13103.
(27) Yang, J. W.; Wang, J.; Zhao, K.; Izuishi, T.; Li, Y.; Shen, Q.; Zhong, X. H. CdSeTe/CdS Type-I Core/Shell Quantum Dot Sensitized Solar Cells with Efficiency over 9%. *J. Phys. Chem. C* **2015**, *119*, 28800−28808.
(28) Zeng, Q. S.; Chen, Z. L.; Zhao, Y.; Du, X. H.; Liu, F. Y.; Jin, G.; Dong, F. X.; Zhang, H.; Yang, B. Aqueous-Processed Inorganic Thin-Film Solar Cells Based on $CdSe_xTe_{1-x}$ Nanocrystals: The Impact of Composition on Photovoltaic Performance. *ACS Appl. Mater. Interfaces* **2015**, *7*, 23223−23230.
(29) Zhu, Z. L.; Cui, L.; Ling, T.; Qiao, S. Z.; Du, X. W. CdTe Nanoflake Arrays on a Conductive Substrate: Template Synthesis and Photoresponse Property. *J. Mater. Chem. A* **2014**, *2*, 957−961.
(30) Meyer, B. K.; Polity, A.; Farangis, B.; He, Y.; Hasselkamp, D.; Kramer, T.; Wang, C. Structural Properties and Bandgap Bowing of $ZnO_{1-x}S_x$ Thin Films Deposited by Reactive Sputtering. *Appl. Phys. Lett.* **2004**, *85*, 4929−4931.
(31) Galian, R. E.; Diaz, P.; Ribera, A.; Rincon-Bertolin, A.; Agouram, S.; Perez-Prieto, J. Controlled Building of CdSe@ZnS/Au and CdSe@ZnS/Au_2S/Au Nanohybrids. *Nano Res.* **2015**, *8*, 2271−2287.
(32) Aldeek, F.; Balan, L.; Medjahdi, G.; Roques-Carmes, T.; Malval, J. P.; Mustin, C.; Ghanbaja, J.; Schneider, R. Enhanced Optical Properties of Core/Shell/Shell CdTe/CdS/ZnO Quantum Dots Prepared in Aqueous Solutionb. *J. Phys. Chem. C* **2009**, *113*, 19458−19467.
(33) Hannachi, L.; Bouarissa, N. Electronic Structure and Optical Properties of $CdSe_xTe_{1-x}$ Mixed Crystals. *Superlattices Microstruct.* **2008**, *44*, 794−801.
(34) El-Nahass, M. M.; Sallam, M. M.; Afifi, M. A.; Zedan, I. T. Structural and Optical Properties of Polycrystalline $CdSe_xTe_{1-x}$ ($0 \leq x \leq 0.4$) Thin Films. *Mater. Res. Bull.* **2007**, *42*, 371−384.
(35) MacDonald, B. I.; Martucci, A.; Rubanov, S.; Watkins, S. E.; Mulvaney, P.; Jasieniak, J. J. Layer-by-Layer Assembly of Sintered $CdSe_xTe_{1-x}$ Nanocrystal Solar Cells. *ACS Nano* **2012**, *6*, 5995−6004.
(36) Muthukumarasamy, N.; Balasundaraprabhu, R.; Jayakumar, S.; Kannan, M. D. Investigations on Structural Phase Transition in Hot Wall Deposited $CdSe_xTe_{1-x}$ Thin Films. *Mater. Chem. Phys.* **2007**, *102*, 86−91.
(37) Ikram, A.; Sahai, S.; Rai, S.; Dass, S.; Shrivastav, R.; Satsangi, V. R. Synergistic Effect of CdSe Quantum Dots on Photoelectrochemical Response of Electrodeposited Alpha-Fe_2O_3 Films. *J. Power Sources* **2014**, *267*, 664−672.
(38) Jung, M. H.; Kang, M. G. Enhanced Photo-Conversion Efficiency of CdSe-ZnS Core-Shell Quantum Dots with Au Nanoparticles on TiO_2 Electrodes. *J. Mater. Chem.* **2011**, *21* (8), 2694−2700.
(39) Windisch, C. F.; Exarhos, G. J. Mott-Schottky Analysis of Thin ZnO Films. *J. Vac. Sci. Technol., A* **2000**, *18*, 1677−1680.
(40) Meissner, D.; Memming, R.; Kastening, B. Photoelectrochemistry of Cadmium Sulfide. 1. Reanalysis of Photocorrosion and Flat-band Potential. *J. Phys. Chem.* **1988**, *92* (12), 3476−3483.
(41) Mathew, X.; Bansal, A.; Turner, J. A.; Dhere, R.; Mathews, N. R.; Sebastian, P. J. Photoelectrochemical Characterization of Surface Modified CdTe for Hydrogen Production. *J. New Mater. Electrochem. Syst.* **2002**, *5* (2), 149−154.
(42) Das, S. K.; Morris, G. C. Preparation and Properties of Electrodeposited Indium Tin oxide/SnO_2/CdTe and Indium Tin Oxide/SnO_2/CdS/CdTe Solar Cells. *J. Appl. Phys.* **1993**, *73* (2), 782.
(43) Sambur, J. B.; Parkinson, B. A. Size Selective Photoetching of CdSe Quantum Dot Sensitizers on Single-Crystal TiO_2. *ACS Appl. Mater. Interfaces* **2014**, *6*, 21916−21920.
(44) Zhou, M.; Bao, J.; Xu, Y.; Zhang, J. J.; Xie, J. F.; Guan, M. L.; Wang, C. L.; Wen, L. Y.; Lei, Y.; Xie, Y. Photoelectrodes Based upon Mo: $BiVO_4$ Inverse Opals for Photoelectrochemical Water Splitting. *ACS Nano* **2014**, *8*, 7088−7098.

DOI: 10.1021/acs.langmuir.7b00878
Langmuir 2017, 33, 6457−6463